Heliyon

Received:
8 February 2017
Revised:
5 June 2017
Accepted:
15 August 2017

Cite as: Daisuke Sato, Colleen E. Clancy, Donald M. Bers. Dynamics of sodium current mediated early afterdepolarizations. Heliyon 3 (2017) e00388.
doi: 10.1016/j.heliyon.2017.e00388

Dynamics of sodium current mediated early afterdepolarizations

Daisuke Sato *, Colleen E. Clancy, Donald M. Bers

Department of Pharmacology, University of California, Davis, CA, United States

* Corresponding author at: Department of Pharmacology, Genome Building (GBSF), University of California, Davis, CA 95616-8636, United States.

E-mail address: dsato@ucdavis.edu (D. Sato).

Abstract

Early afterdepolarizations (EADs) have been attributed to two primary mechanisms: 1) recovery from inactivation of the L-type calcium (Ca) channel and/or 2) spontaneous Ca release, which depolarizes the membrane potential through the electrogenic sodium-calcium exchanger (NCX). The sodium (Na) current (I_{Na}), especially the late component of the Na current, has been recognized as an important player to set up the conditions for EADs by reducing repolarization reserve and increasing intracellular Na concentration, which leads to Ca overload. However, I_{Na} itself has not been considered as a direct initiator of EADs. A recent experimental study by Horvath et al. has shown that the amplitude of the late component of the Na current is as large as potassium (K) and Ca currents (~1 pA/pF). This result suggests that I_{Na} by itself can exceeds the sum of outward currents and depolarize the membrane potential. In this study, we show that I_{Na} can also directly initiate EADs. Mathematical analysis reveals a fundamental dynamical origin of EADs arising directly from the Na channel reactivation. This system has three fixed points. The dynamics of the I_{Na} mediated EAD oscillation is different from that of the membrane voltage oscillation of the pacemaker cell, which has only one fixed point.

Keywords: Medicine, Applied mathematics, Systems biology, Cell biology, Physiology, Cardiology, Biophysics

http://dx.doi.org/10.1016/j.heliyon.2017.e00388

1. Introduction

Cardiac arrhythmia is often triggered by premature ventricular contractions (PVCs), which have been linked to early afterdepolarizations (EADs) [1, 2, 3, 4, 5]. EADs have been thought to be caused by reactivation of the L-type calcium (Ca) channel or spontaneous Ca releases from the sarcoplasmic reticulum (SR), which depolarize the membrane potential (V_m) via the electrogenic sodium(Na)-Ca exchanger (NCX) [6, 7, 8, 9, 10, 11, 12, 13]. During the upstroke (phase 0) of the action potential (AP), Na channel opening gives large but extremely short (~1 ms) inward current [14]. Then, immediately following the upstroke, the Na channel goes to the inactivated state. At the plateau phase of AP, the amplitude of Na current (I_{Na}) is thought to be much smaller than the other currents and the shape and the duration of AP are mainly determined by the other currents such as the L-type Ca current (I_{CaL}), NCX, and potassium (K) currents [15]. Na channel mutations have been associated with long QT syndrome by increasing window current and non-inactivating current [16, 17, 18]. Recent experimental measurement by Horvath et al. has shown that the amplitude of I_{Na} at phases 2 and 3 of AP ('late component of the Na current' or simply 'late Na current') can be surprisingly large and of similar amplitude to outward K currents [19]. This implies that the inward current via I_{Na} may become larger than the sum of outward currents and V_m can be depolarized. In this study, using a physiologically detailed model of a cardiac ventricular myocyte, we show that I_{Na} not only sets up the conditions for EADs by reducing repolarization reserve and increasing intracellular Na concentration, which leads to Ca overload, but also can directly initiate EADs. Mathematical reduction of the detailed model was then performed to generate 2- and 3-variable models, whose variables are membrane potential, inactivation of the Na channel, and the K conductance (for the third variable of the 3-variable model). Analysis in the reduced models reveals a fundamental dynamical origin of EADs arising directly from the Na channel reactivation, as oscillations of V_m at phases 2 and/or 3 of AP. Oscillatory behavior has also been extensively investigated in neuron [20, 21, 22] and pacemaker cells [23, 24]. We show that these ventricular myocyte EADs have a different dynamical mechanism from those of pacemaker cell V_m oscillation.

2. Materials and methods

2.1. Mathematical formulation

We use a physiologically detailed mathematical model of the rabbit ventricular action potential by Mahajan *et al.* [25]. The membrane voltage is governed by

$$\frac{dV}{dt} = -\frac{\sum I}{C_m},$$

http://dx.doi.org/10.1016/j.heliyon.2017.e00388

where V is the membrane voltage, C_m is the cell capacitance, I represents the transmembrane currents. The details of the mathematical model are described in the next section.

There are several proposed mechanisms of the late component of I_{Na} [16, 17, 18]. In this study we consider two mechanisms; (1) large window current mechanism and (2) non-inactivating current mechanism.

In order to increase the window current, activation and inactivation curves are shifted (Fig. 1A). The formula for I_{Na} is

$$I_{Na} = G_{Na} mhj(\mathrm{V} - E_{Na}),$$

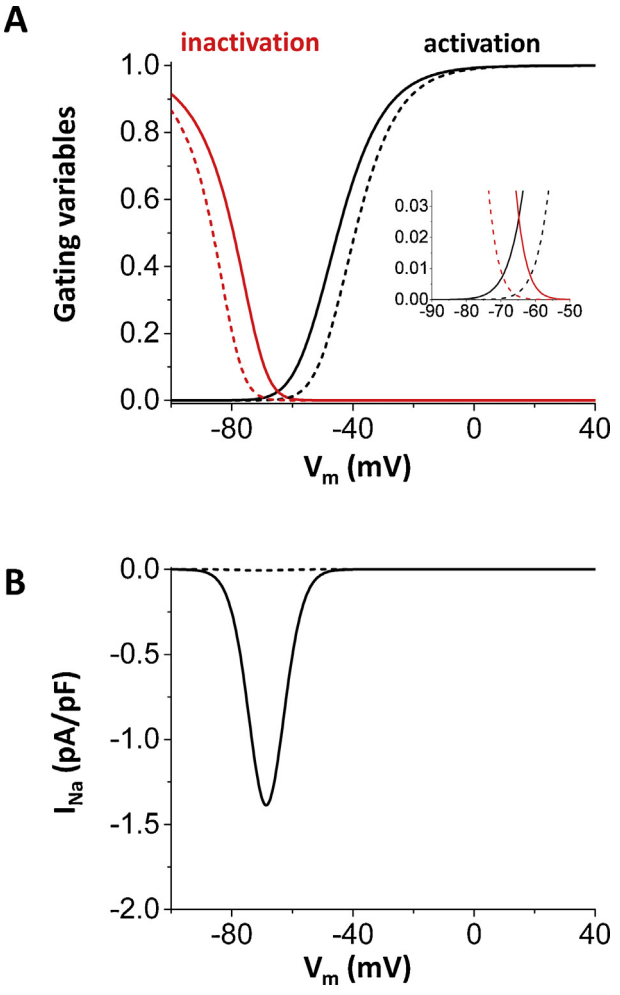

Fig. 1. Normal Na current and pathological (increased late component of I_{Na}) Na current. (A) Activation and inactivation curves. Activation curve is m^3 and inactivation curve is $h \times j$. Solid lines: Increased window for the late component of I_{Na}. Dashed lines: normal Na channel. (B) Steady state current. Solid lines: Na current with the increased window. Dashed lines: normal Na current.

http://dx.doi.org/10.1016/j.heliyon.2017.e00388

where G_{Na} is the maximum conductance, E_{Na} is the reversal potential given by $RT/F\log\left([Na]_o/[Na]_i\right)$, where R is the gas constant, T is the temperature, F is the Faraday constant, $[Na]_o$ is the outside Na concentration, $[Na]_i$ is the cytosolic Na concentration. m is the Na activation and h and j are the fast and slow Na inactivation, respectively. The window current of I_{Na} was increased so that the peak of the 'window' becomes about 2–3 percent based on the experimental observations (Fig. 1A inset) [26]. Here we note that in the major mathematical models including Mahajan et al. model, Luo-Rudy passive model (LR1) [27], Luo-Rudy dynamic model (LRd) [28], and Shannon-Bers model [29], the peak V_m of the window is higher (−50 to −60 mV) than that in the experimental observations (−60 to –70 mV) [26]. Therefore, we shifted the curves so that the peak V_m of the window correspond reasonably well with the experimental measurements [26]. In order to shift the window, activation and inactivation are changed as follows.

$$\alpha_m = \left(0.32\frac{V+127.13}{1-\exp(-0.1(\mathrm{V}+127.13))}\right),$$

$$\beta_m = 0.08\exp\left(-\frac{V}{11}\right),$$

$$\alpha_h = \frac{3.5\exp\left(\frac{V+100}{-23}\right)}{1+\exp(0.15(V+79))},$$

$$\beta_h = \left(\frac{6.0}{1+\exp(-0.05(V+32))}\right),$$

$$\alpha_j = \frac{0.175\exp\left(\frac{V+100}{-23}\right)}{1+\exp(0.15(V+79))},$$

$$\beta_j = \left(\frac{0.3}{1+\exp(-0.05(V+32))}\right).$$

The difference between the h gate and the j gate is the time constant. The j gate is 20 times slower than the h gate.

In order to simulate non-inactivating current, we assumed 1% of channels are non-inactivating (smallest value of h (and j) is 0.1) gates are always open regardless of V_m). The activation curve and the inactivation curve are show in Fig. 6A.

The physiologically detailed model has 26 variables. We reduce the number of variables in order to analyze the dynamical mechanism of EADs. We show the mechanism of oscillations of V_m i.e. EADs using the 2-variable model and the mechanism of termination of EADs using the 3-variable model.

2.2. Mathematical model (detailed description)

Our base model is an AP model by Mahajan et al. [25]. The ordinary differential equations are solved by the Euler method with adaptive time step of 0.01–0.1 ms.

http://dx.doi.org/10.1016/j.heliyon.2017.e00388

The program codes are written in C++. Parameters are shown in Tables 1–6 . Equations are as follows.

2.3. Ionic currents

The membrane voltage (V_m) is given by

$$\frac{dV}{dt} = -\frac{I_{ion} + I_{stim}}{C_m},$$

where $C_m = 1$ μF/cm^2 is membrane capacitance, I_{ion} is total ionic current density across the cell membrane, and I_{stim} is the stimulus current. The total membrane current is given by

$$I_{ion} = I_{Na} + I_{to,f} + I_{to,s} + I_{Kr} + I_{Ks} + I_{K1} + I_{NaK} + I_{Ca} + I_{NaCa}$$

2.4. The sodium current (I_{Na})

We modified the original Mahajan formulation so that the peak V_m of the window corresponds reasonably well with the experimental measurements [26].

I_{Na} is given by

$$I_{Na} = G_{Na} mhj(V - E_{Na}),$$

Na channel activation for the large window current is given by

$$\frac{dm}{dt} = (m_\infty - m)/\tau_m,$$

$$m_\infty = \frac{\alpha_m}{\alpha_m + \beta_m},$$

$$\tau_m = \frac{1}{\alpha_m + \beta_m},$$

Table 1. SR release parameters.

Parameter	Definition	Value
τ_r	Spark lifetime	30 ms
τ_a	NSR-JSR relaxation time	100 ms
g_{RyR}	Release current strength	2.58 sparks cm^2/mA
u	Release slope	11.3 ms^{-1}
c_{sr}	Threshold for steep release function	90 μM/l cytosol
s	Release function parameter	−977 μM/ms
τ_d	Submembrane-myoplasm diffusion time constant	4 ms
τ_s	Dyadic junction-submembrane diffusion time constant	0.5 ms

http://dx.doi.org/10.1016/j.heliyon.2017.e00388

Table 2. Cytosolic buffering parameters.

Parameter	Definition	Value
B_T	Total concentration of Troponin C	70 μmol/l cytosol
B_{SR}	Total concentration of SR binding sites	47 μmol/l cytosol
B_{Cd}	Total concentration of Calmodulin binding sites	24 μmol/l cytosol
B_{mem}	Total concentration of membrane binding sites	15.0 μmol/l cytosol
B_{sar}	Total concentration of sarcolemma binding sites	42.0 μmol/l cytosol
$k_{on}{}^{T}$	On rate for Troponin C binding	0.0327 $(\mu M)^{-1}(ms)^{-1}$
$k_{off}{}^{T}$	Off rate for Troponin C binding	0.0196 ms^{-1}
K_{SR}	Dissociation constant for SR binding sites	0.6 μM
K_{Cd}	Dissociation constant for Calmodulin binding sites	7 μM
$K_{\ mem}$	Dissociation constant for membrane binding sites	0.3 μM
$K_{\ sar}$	Dissociation constant for sarcolemma binding sites	13.0 μM

$$\alpha_m = \left(0.32\frac{V + 102.13}{1 - \exp(-0.1(\mathrm{V} + 102.13))}\right),$$

$$\beta_m = 0.08\exp\left(-\frac{V}{11}\right),$$

Na channel inactivation for the large window current is given by

$$\frac{dh}{dt} = (h_\infty - h)/\tau_h,$$

Table 3. Exchanger, uptake, and SR leak parameters.

Parameter	Definition	Value
c_{up}	Uptake threshold	0.5 μM
v_{up}	Strength of Uptake	0.4 μM/ms
g_{NaCa}	Strength of exchange current	0.84 μM/s
k_{sat}	constant	0.2
ξ	constant	0.35
$K_{m,Nai}$	constant	12.3 mM
$K_{m,Nao}$	constant	87.5 mM
$K_{m,Cai}$	constant	0.0036 mM
$K_{m,Cao}$	constant	1.3 mM
c_{naca}	constant	0.3 μM
g_l	Strength of leak current	2.07×10^{-5} $(ms)^{-1}$
k_j	Threshold for leak onset	50 μM

http://dx.doi.org/10.1016/j.heliyon.2017.e00388

Table 4. L-type Ca current parameters.

Parameter	Definition	Value
P_{Ca}	Constant	0.00054 cm/s
g_{Ca}	Strength of Ca current flux	182 mmol/(cm C)
$\overline{g}_{Ca}$	Strength of local Ca flux due to L-type Ca channels	9000 mmol/(cm C)
$\overline{g}_{SR}$	Strength of local Ca flux due to RyR channels	26842 mmol/(cm C)
k_p°	Threshold for Ca-induced inactivation	3.0 μM
$\overline{c}_p$	Threshold for Ca dependence of transition rate k_6	6.1 μM
τ_{po}	Time constant of activation	1 ms
r_1	Opening rate	0.3 ms^{-1}
r_2	Closing rate	3 ms^{-1}
s_1'	Inactivation rate	0.00195 ms^{-1}
k_1'	Inactivation rate	0.00413 ms^{-1}
k_2	Inactivation rate	0.0001 ms^{-1}
k_{21}'	Inactivation rate	0.00224 ms^{-1}
T_{Ba}	Time constant	450 ms

$$h_\infty = \frac{\alpha_h}{\alpha_h + \beta_h},$$

$$\tau_h = \frac{1}{\alpha_h + \beta_h},$$

Table 5. Physical constants and ionic concentrations.

Parameter	Definition	Value
C_m	Cell capacitance	3.1×10^{-4} μF
v_i	Cell volume	2.58×10^{-5} μl
v_s	Submembrane volume	0.02 v_i
F	Faraday constant	96.5C/mmol
R	Universal gas constant	8.315 J $mol^{-1}K^{-1}$
T	Temperature	308 K
$[Na^+]_o$	External sodium concentration	136 mM
$[K^+]_i$	Internal potassium concentration	140 mM
$[K^+]_o$	External potassium concentration	5.4 mM
$[Ca^{2+}]_o$	External calcium concentration	1800 μM

http://dx.doi.org/10.1016/j.heliyon.2017.e00388

Table 6. Ion current conductances.

Parameter	Definition	Value
g_{Na}	Peak I_{Na} conductance	12.0 mS/μF
$g_{to,f}$	Peak $I_{to,f}$ conductance	0.11 mS/μF
$g_{to,s}$	Peak $I_{to,s}$ conductance	0.04 mS/μF
g_{K1}	Peak I_{K1} conductance	0.3 mS/μF
g_{Kr}	Peak I_{Kr} conductance	0.0125 mS/μF
g_{Ks}	Peak I_{Ks} conductance	0.1386 mS/μF
g_{NaK}	Peak I_{NaK} conductance	1.5 mS/μF

$$\alpha_h = \frac{3.5\exp\left(\frac{V+95}{-23}\right)}{1+\exp(0.15(V+74))},$$

$$\beta_h = \left(\frac{6.0}{1+\exp(-0.05(V+32))}\right),$$

$$\frac{dj}{dt} = (j_\infty - j)/\tau_j,$$

$$j_\infty = \frac{\alpha_j}{\alpha_j+\beta_j},$$

$$\tau_j = \frac{1}{\alpha_j+\beta_j},$$

$$\alpha_j = \frac{0.175\exp\left(\frac{V+95}{-23}\right)}{1+\exp(0.15(V+74))},$$

$$\beta_j = \left(\frac{0.3}{1+\exp(-0.05(V+32))}\right).$$

On the other hand, normal Na channel activation is given by

$$\frac{dm}{dt} = (m_\infty - m)/\tau_m,$$

$$m_\infty = \frac{\alpha_m}{\alpha_m+\beta_m},$$

$$\tau_m = \frac{1}{\alpha_m+\beta_m},$$

$$\alpha_m = \left(0.32\frac{v+72.13}{1-\exp(-0.1(V+72.13))}\right),$$

$$\beta_m = 0.08\exp\left(-\frac{V}{11}\right),$$

http://dx.doi.org/10.1016/j.heliyon.2017.e00388

Normal Na channel inactivation is given by

$$\frac{dh}{dt} = (h_\infty - h)/\tau_h,$$

$$h_\infty = \frac{\alpha_h}{\alpha_h + \beta_h},$$

$$\tau_h = \frac{1}{\alpha_h + \beta_h},$$

$$\alpha_h = \frac{3.5\exp\left(\frac{V+105}{-23}\right)}{1 + \exp(0.15(V+84))},$$

$$\beta_h = \left(\frac{6.0}{1 + \exp(-0.05(V+32))}\right),$$

$$\frac{dj}{dt} = (j_\infty - j)/\tau_j,$$

$$j_\infty = \frac{\alpha_j}{\alpha_j + \beta_j},$$

$$\tau_j = \frac{1}{\alpha_j + \beta_j},$$

$$\alpha_j = \frac{0.175\exp\left(\frac{V+105}{-23}\right)}{1 + \exp(0.15(V+84))},$$

$$\beta_j = \left(\frac{0.3}{1 + \exp(-0.05(V+32))}\right).$$

2.5. Inward rectifier K^+ current (I_{K1})

I_{K1} is given by

$$I_{K1} = g_{K1}\sqrt{\frac{[K^+]_o}{5.4}}\frac{A_{K1}}{A_{K1} + B_{K1}}(V - E_K)$$

$$A_{K1} = \frac{1.02}{1.0 + e^{0.2385(V - E_K - 59.215)}}$$

$$B_{K1} = \frac{0.49124e^{0.08032(V - E_K + 5.476)} + e^{0.061750(V - E_K - 594.31)}}{1 + e^{-0.5143(V - E_K + 4.753)}}$$

$$E_K = \frac{RT}{F}\ln\left(\frac{[K^+]_o}{[K^+]_i}\right).$$

http://dx.doi.org/10.1016/j.heliyon.2017.e00388

2.6. The rapid component of the delayed rectifier K^+ current (I_{Kr})

I_{Kr} is given by

$$I_{Kr} = g_{Kr}\sqrt{\frac{[K^+]_o}{5.4}}x_{Kr}R(V)(V - E_K)$$

$$R(V) = \frac{1}{1 + e^{(V+33)/22.4}}$$

$$\frac{dx_{Kr}}{dt} = \frac{x_{Kr}^{\infty} - x_{Kr}}{\tau_{Kr}}$$

$$x_{Kr}^{\infty} = \frac{1}{1 + e^{-(V+50)/7.5}}$$

$$\tau_{Kr} = \frac{1}{\left(\frac{0.00138(V+7)}{1-e^{-0.123(V+7)}} + \frac{0.00061(V+10)}{-1+e^{0.145(V+10)}}\right)}$$

2.7. The slow component of the delayed rectifier K^+ current (I_{Ks})

I_{Ks} is given by

$$I_{Ks} = g_{Ks}x_{s1}x_{s2}q_{Ks}(V - E_{Ks})$$

$$q_{Ks} = 1 + \frac{0.8}{\left(1 + \left(\frac{0.5}{c_i}\right)^3\right)}$$

$$\frac{dx_{s1}}{dt} = \frac{x_x^{\infty} - x_{s1}}{\tau_{xs1}}$$

$$\frac{dx_{s2}}{dt} = \frac{x_x^{\infty} - x_{s2}}{\tau_{xs2}}$$

$$x_s^{\infty} = \frac{1}{1 + e^{-(V-1.5)/16.7}}$$

$$\tau_{xs1} = \frac{1}{\left(\frac{0.0000719(V+30)}{1-e^{-0.148(V+30)}} + \frac{0.00031(V+30)}{-1+e^{0.0687(V+30)}}\right)}$$

$$\tau_{xs2} = 4\tau_{xs1}$$

$$E_{Ks} = \frac{RT}{F}\ln\left(\frac{[K^+]_o + 0.01833[Na^+]_o}{[K^+]_i + 0.01833[Na^+]_i}\right).$$

http://dx.doi.org/10.1016/j.heliyon.2017.e00388

2.8. The NaK exchanger current (I_{NaK})

I_{NaK} is given by

$$\sigma = \frac{e^{[Na^+]_o/67.3} - 1}{7}$$

$$f_{NaK} = \frac{1}{1 + 0.1245e^{-0.1VF/RT} + 0.0365\sigma e^{-VF/RT}}$$

$$I_{NaK} = g_{NaK} f_{NaK} \left(\frac{1}{1 + \left(12mM/[Na^+]_i\right)} \right) \left(\frac{[K^+]_o}{[K^+]_o + 1.5mM} \right).$$

2.9. The fast component of the rapid inward K^+ current ($I_{to,f}$)

$I_{to,f}$ is given by

$$I_{to,f} = g_{to,f} X_{to,f} Y_{to,f} (V - E_K)$$

$$X^{\infty}_{to,f} = \frac{1}{1 + e^{-(V+3)/15}}$$

$$Y^{\infty}_{to,f} = \frac{1}{1 + e^{(V+33.5)/10}}$$

$$\tau_{Xto,f} = 3.5e^{-(V/30)} + 1.5$$

$$\tau_{Yto,f} = \frac{20}{1 + e^{(V+33.5)/10}} + 20$$

$$\frac{dX_{to,f}}{dt} = \frac{X^{\infty}_{to,f} - X_{to,f}}{\tau_{Xto,f}}$$

$$\frac{dY_{to,f}}{dt} = \frac{Y^{\infty}_{to,f} - Y_{to,f}}{\tau_{Yto,f}}$$

2.10. The slow component of the rapid outward K^+ current ($I_{to,s}$)

$I_{to,s}$ is given by

$$I_{to,s} = g_{to,s} X_{to,s} \left(Y_{to,s} + 0.5R^{\infty}_s\right)(V - E_K)$$

$$R^{\infty}_s = \frac{1}{1 + e^{(V+33.5)/10}}$$

$$X^{\infty}_{to,s} = \frac{1}{1 + e^{-(V+3)/15}}$$

$$Y^{\infty}_{to,s} = \frac{1}{1 + e^{(V+33.5)/10}}$$

$$\tau_{Xto,s} = 9/\left(1 + e^{(V+3)/15}\right) + 0.5$$

http://dx.doi.org/10.1016/j.heliyon.2017.e00388

$$\tau_{Yto,s} = \frac{3000}{1 + e^{(V+60)/10}} + 30$$

$$\frac{dX_{to,s}}{dt} = \frac{X^{\infty}_{to,s} - X_{to,s}}{\tau_{Xto,f}}$$

$$\frac{dY_{to,s}}{dt} = \frac{Y^{\infty}_{to,s} - Y_{to,s}}{\tau_{Yto,s}}$$

2.11. Equations for Ca cycling

The equations for Ca cycling are:

$$\frac{dc_s}{dt} = \beta_s \left[\frac{v_i}{v_s}(J_{rel} - J_d + J_{Ca} + J_{NaCa}) - J^s_{trpn} \right],$$

$$\frac{dc_i}{dt} = \beta_i \left[J_d - J_{up} + J_{leak} - J^i_{trpn} \right],$$

$$\frac{dc_j}{dt} = -J_{rel} + J_{up} - J_{leak},$$

$$\frac{dc_j^{'}}{dt} = \frac{c_j - c_j^{'}}{\tau_a},$$

$$\frac{dJ_{rel}}{dt} = N_s^{'}(t) C c_j C \frac{Q\left(c_j^{'}\right)}{c_{sr}} - \frac{J_{rel}}{T},$$

$$T = \frac{\tau_r}{1 - \tau_r \frac{\frac{dc_j}{dt}}{c_j}},$$

where c_s, c_i, and c_j are free [Ca] in the submembrane space, the cytosol, and the SR, with volumes v_s, v_i and v_{sr}respectively. The concentrations c_s and $c_i$are in units of μM, whereas c_j and c_j' (for simplicity) are both in units of μMv_{sr}/v_i (μM/l cytosol). The current fluxes are: J_{rel}, the total release flux out of the SR via RyR channels; J_d, diffusion of Ca from the submembrane space to the bulk myoplasm; J_{up}, the uptake current via SERCA pumps in the SR; J_{Ca}, the current flux into the cell via L-type Ca channels; J_{NaCa}, the current flux into the cell via the NaCa exchanger; J_{leak}, the leak current from the SR into the bulk myoplasm. All Ca fluxes are divided by v_i and have units of μM/ms, which can be converted to units of μA/μF using the conversion factor nFv_i/C_m, where n is the ionic charge of the current carrier, C_m is the cell membrane capacitance, and where F is Faraday's constant. Ionic fluxes can be converted to membrane currents using

$$I_{Ca} = -2\alpha J_{Ca},$$
$$I_{NaCa} = \alpha J_{NaCa},$$

where α = Fv_i/C_m, and where the ion currents are in units of μA/μF.

http://dx.doi.org/10.1016/j.heliyon.2017.e00388

The dependence of Ca release on SR Ca load is given by

$$Qc_j^{'} = \begin{cases} 0, & 0 < c_j^{'} < 50, \\ c_j^{'} - 50, & 50 \le c_j^{'} \le c_{sr}, \\ uc_j^{'} + s, & c_j^{'} > c_{sr}, \end{cases}$$

where the parameter u controls the slope of the SR Ca release vs. SR Ca load relationship at high loads (c_j' > c_{sr}). The parameter s is chosen so that the function $Q(c_j$') is continuous at c_{sr}.

The number of sparks recruited over the whole cell in a time interval Δt is given by ΔN_s, and the rate of spark recruitment is N_s' = $\Delta N_s/\Delta t$. Since spark recruitment is initiated by the stochastic single channel opening of L-type Ca channels distributed throughout the cell, N_s' follows a voltage dependence similar to the whole cell Ca entry. A phenomenological expression for spark rate is given by

$$N_s^{'} = -g_{RyR}(V)P_o i_{Ca},$$

where $g(V)$ is the gain function, which controls the voltage dependence of Ca released into the SR in response to a trigger from the L-type Ca current. The voltage dependence is weak and has the form

$$g_{RyR}(V) = g_{RyR}\frac{e^{-0.05(V+30)}}{1+e^{-0.05(V+30)}}.$$

2.12. The L-type Ca current flux

The Ca flux into the cell due to the L-type Ca current is given by

$$J_{Ca} = g_{Ca}P_o i_{Ca},$$

$$i_{Ca} = \frac{4P_{Ca}VF^2c_s e^{2a} - 0.341\left[Ca^{2+}\right]_o}{RT \qquad e^{2a}-1},$$

where $\alpha = VF/RT$, and where c_s is the submembrane concentration in units of mM.

2.13. Markov model of the L-type Ca current

The equations for the Markov states of L-type Ca channels are:

$$\frac{dC_2}{dt} = \beta C_1 + k_5 I_{2Ca} + k_5^{'} I_{2Ba} - \left(k_6 + k_6^{'} + \alpha\right)C_2,$$

$$\frac{dC_1}{dt} = \alpha C_2 + k_2 I_{1Ca} + k_2^{'} I_{1Ba} + r_2 P_o - \left(r_1 + \beta + k_1 + k_1^{'}\right)C_1,$$

$$\frac{dI_{1Ca}}{dt} = k_1 C_1 + k_4 I_{2Ca} + s_1 P_o - (k_2 + k_3 + s_2)I_{1Cao},$$

http://dx.doi.org/10.1016/j.heliyon.2017.e00388

$$\frac{dI_{2Ca}}{dt} = k_3 I_{1Ca} + k_6 C_2 - (k_4 + k_5) I_{2Ca},$$

$$\frac{dI_{1Ba}}{dt} = k_1^{'} C_1 + k_4^{'} I_{2Ba} + s_1^{'} P_o - \left(k_2^{'} + k_3^{'} + s_2^{'}\right) I_{1Ba},$$

$$\frac{dI_{2Ba}}{dt} = k_3^{'} I_{1Ba} + k_6^{'} C_2 - \left(k_5^{'} + k_4^{'}\right) I_{2Ba},$$

where the open probability satisfies

$$P_o = 1 - (C_1 + C_2 + I_{1Ca} + I_{2Ca} + I_{1Ba} + I_{2Ba}).$$

The rates are given by:

$$\alpha = p_o^{\infty} / \tau_{po},$$

$$\beta = \left(1 - p_o^{\infty}\right) / \tau_{po},$$

$$p_o^{\infty} = \frac{1}{1 + e^{-V/8}},$$

$$s_1 = 0.02 f\left(c_p\right),$$

$$k_1 = 0.03 f\left(c_p\right),$$

$$s_2 = s_1 (k_2 / k_1)(r_1 / r_2),$$

$$s_2^{'} = s_1^{'} \left(k_2^{'} / k_1^{'}\right)(r_1 / r_2),$$

$$f\left(c_p\right) = \frac{1}{1 + \left(\frac{\tilde{c_p}}{c_p}\right)^3}$$

$$k_3 = \frac{e^{-(V+40)/3}}{3(1 + e^{-(V+40)/3})},$$

$$k_3^{'} = k_3,$$

$$k_4 = k_3 (\alpha / \beta)(k_1 / k_2)(k_5 / k_6),$$

$$k_4^{'} = k_3^{'} (\alpha / \beta) \left(k_1^{'} / k_2^{'}\right) \left(k_5^{'} / k_6^{'}\right),$$

$$k_5 = (1 - P_s) / \tau_{Ca},$$

$$k_6 = f\left(c_p\right) P_s / \tau_{Ca},$$

$$k_5^{'} = (1 - P_s) / \tau_{Ba},$$

$$k_6^{'} = P_s / \tau_{Ba},$$

$$\tau_{Ca} = (R(V) - T_{Ca}) P_r + T_{Ca}$$

$$\tau_{Ba} = (R(V) - T_{Ba}) P_r + T_{Ba}$$

 http://dx.doi.org/10.1016/j.heliyon.2017.e00388

$$T_{Ca} = \frac{114}{1 + \left(\frac{c_p}{\overline{c_p}}\right)^4}$$

$$R(V) = 10 + 4954e^{V/15.6}$$

$$P_r = \frac{e^{-(V+40)/4}}{1 + e^{-(V+40)/4}}$$

$$P_s = \frac{e^{-(V+40)/11.32}}{1 + e^{-(V+40)/11.32}}$$

2.14. Diffusive flux

The flux of Ca from the submembrane space to the bulk myoplasm is given by:

$$J_d = \frac{c_s - c_i}{\tau_d},$$

where τ_d is the time constant for Ca diffusion from the submembrane space to the bulk myoplasm.

2.15. Nonlinear buffering

Buffering of Ca is modeled by incorporating instantaneous buffering to SR, calmodulin, membrane and sarcolemma binding sites.

$$\beta_s = \left(1 + \frac{B_{SR}K_{SR}}{(c_s + K_{SR})^2} + \frac{B_{cd}K_{cd}}{(c_s + K_{cd})^2} + \frac{B_{mem}K_{mem}}{(c_s + K_{mem})^2} + \frac{B_{sar}K_{sar}}{(c_s + K_{sar})^2}\right)^{-1},$$

$$\beta_i = \left(1 + \frac{B_{SR}K_{SR}}{(c_i + K_{SR})^2} + \frac{B_{cd}K_{cd}}{(c_i + K_{cd})^2} + \frac{B_{mem}K_{mem}}{(c_i + K_{mem})^2} + \frac{B_{sar}K_{sar}}{(c_i + K_{sar})^2}\right)^{-1}.$$

Time dependent buffering to Troponin C is described by

$$\frac{d[CaT]_i}{dt} = J^i_{trpn},$$

$$\frac{d[CaT]_s}{dt} = J^s_{trpn},$$

$$J^i_{trpn} = k^T_{on}c_i\left(B_T - [CaT]_i\right) - k^T_{off}[CaT]_i$$

$$J^s_{trpn} = k^T_{on}c_s\left(B_T - [CaT]_s\right) - k^T_{off}[CaT]_s.$$

http://dx.doi.org/10.1016/j.heliyon.2017.e00388

2.16. NCX flux

The equation of the NCX is given by

$$J_{NaCa} = g_{naca} K_a \frac{e^{\varsigma a}[Na^+]_i^3 \left[Ca^{2+}\right]_o - e^{(\varsigma-1)a}[Na^+]_o^3 c_s}{(1 + k_{sat} e^{(\varsigma-1)a})H}$$

where

$$H = K_{m,Cao}[Na^+]_i^3 + K_{m,Nao}^3 C c_s + K_{m,Nai}^3 \left[Ca^{2+}\right]_o \left(1 + \frac{c_s}{K_{m,Cai}}\right) + K_{m,Cai}[Na^+]_i^3 \left(1 + \frac{[Na^+]_i^3}{K_{m,Nai}^3}\right) + [Na^+]_i^3 \left[Ca^{2+}\right]_o + [Na^+]_i^3 c_s,$$

and where

$$K_a = \frac{1}{1 + \left(\frac{c_{naca}}{c_s}\right)^3}.$$

2.17. The SERCA (uptake) pump

The SERCA Ca pump is given by

$$J_{up} = \frac{v_{up} c_i^2}{c_i^2 + c_{up}^2},$$

where v_{up} denotes the strength of uptake and $c_{up}$is the pump threshold.

2.18. The SR leak flux

The leak flux from the SR is given by

$$J_{leak} = g_l L(c_j) \left(\left(\frac{v_i}{v_{sr}} \right) c_j - c_i \right),$$

where v_{sr}/v_i is the SR to cytoplasm volume ratio, and $L(c_j)$ is a threshold function of the form

$$L(c_j) = \frac{c_j^2}{c_j^2 + k_j^2}$$

2.19. Ca dynamics in the dyadic space

The average concentration in active dyadic clefts is given by

$$\frac{dc_p}{dt} = \tilde{J}_{SR} + \tilde{J}_{Ca} - \frac{c_p - c_s}{\tau_s},$$

where,

http://dx.doi.org/10.1016/j.heliyon.2017.e00388

$$\tilde{J}_{Ca} = -\overline{g}_{Ca} P_o i_{Ca},$$

$$\tilde{J}_{SR} = -g_{SR}(V) Q\left(c_j^{'}\right) P_o i_{Ca},$$

$$\tilde{g}_{SR}(V) = \overline{g}_{SR} e^{-0.356(V+30)} / \left(1 + e^{-0.356(V+30)}\right).$$

2.20. Na dynamics

Intracellular Na dynamics is given by

$$\frac{d[Na^+]_i}{dt} = \frac{1}{\alpha'}(I_{Na} + 3I_{NaCa} + 3I_{NaK})$$

where the factor 1/α' converts membrane currents in μA/μF to Na fluxes in units of mM/ms. The conversion factor is given by α' = 1000α, where $\alpha = Fv_i/C_m$.

3. Results

3.1. EADs directly initiated by I_{Na}

One possible mechanism of the increased late component of I_{Na} is the increased window current mechanism [26, 30, 31]. The peak of the window defined as the cross point of the activation and inactivation curves, which is observed when about 0.16% of Na channels are activated and 0.16% of channels are not inactivated (observed as the value 0.0016 on the ordinal axis in Fig. 1A dashed lines). The conductance at this point is only 0.000256% of the maximum conductance (G_{Na}), and thus the maximum steady state I_{Na} (conductance × (V_m − E_{Na})) is about 0.0057 pA/pF (Fig. 1B dashed line). Note here that the time scale of Na channel inactivation is much shorter (a few ms ~25 ms) than the time scale of AP (>100 ms). Therefore, the steady state approximation is close to the value of the late component of I_{Na} measured during APs.

Next, based on published experimental results for Na channel mutations in the congenital long QT syndrome [26], we shifted the activation curve to lower V_m and inactivation curve to higher V_m so that the peak of the window becomes between 2 to 3 percent (Fig. 1A solid lines). This window of the Na channel is sufficient to increase the amplitude of I_{Na} to ~1.5 pA/pF which is similar to the other K currents at phases 2 and 3 (Fig. 1B solid line).

Using the increased window of I_{Na}, we show examples of EADs (Fig. 2). Fig. 2A shows periodic EADs. Note that action potentials are slightly different from what we usually observe in experiments because the I_{CaL} was completely blocked (G_{CaL} = 0). The main purpose of this figure is to show I_{Na} by itself can generate EADs. Blocking I_{CaL} prevents both EADs due to reactivation of the L-type Ca channel and

http://dx.doi.org/10.1016/j.heliyon.2017.e00388

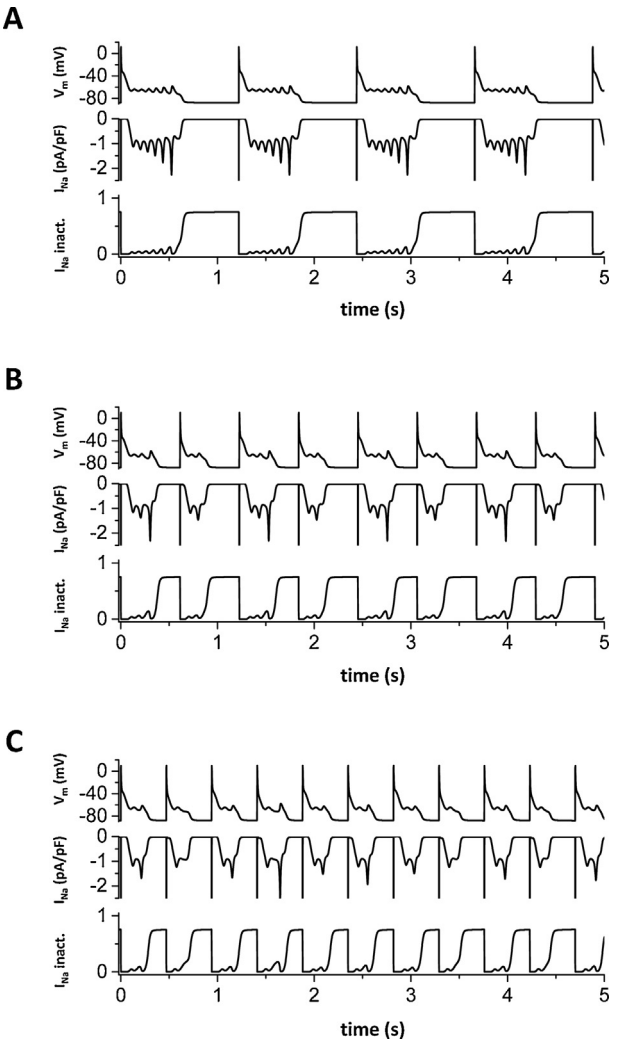

Fig. 2. I_{Na} mediated EADs. Typical EADs due to reactivation of I_{Na} in the physiologically detailed model. I_{CaL} was blocked ($G_{CaL} = 0$) to show explicitly these EADs are due to reactivation of I_{Na}. (A) EADs are periodic when pacing cycle length (PCL) = 1220 ms. (B) EADs show period 2 when PCL = 613 ms. (C) EADs are irregular when PCL is 470 ms. Irregular EADs shown here are sensitive to the initial conditions (see Fig. 3).

spontaneous Ca releases from the SR. Therefore, these EADs are solely due to reactivation of the Na channel as it enters the window current range of V_m. Lower panels in each figure show I_{Na} and inactivation ($h \times j$). These panels show that the Na channel recovers and reactivates along with EADs. These EADs occur around -70 mV, which is lower than the voltage range ($-20 \sim 10$ mV) of EADs due to reactivation of the L-type Ca channel (I_{CaL}-mediated EADs).

Fig. 2B shows period two EADs, that is AP with three EADs and with two EADs appear alternately. Fig. 2C shows irregular EADs. These irregular EADs are probably chaotic since these EADs are sensitive to the initial conditions, which is a hallmark of chaotic systems. (Fig. 3). When two simulations are performed with

http://dx.doi.org/10.1016/j.heliyon.2017.e00388

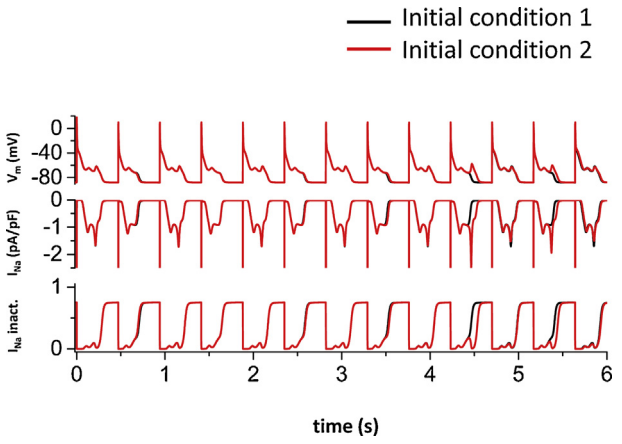

Fig. 3. Sensitivity to initial conditions. Irregular EADs with slightly different initial conditions (initial V_m in the second simulation (Red line) is 1 mV higher (−86.9 mV) than the first simulation (−87.9 mV) (Black line).

slightly different initial conditions, both APs are initially very similar. However, after a couple of beats (about 10 beats in Fig. 3), APs became completely different.

In this study, we used the ventricular cell model. The cell remains excitable around −86 mV and V_m stays at the resting potential if there is no external stimulus. This dynamical behavior is clearly different from that of the pacemaker cell, which is oscillatory without stimuli [23, 24].

3.2. Mathematical analysis

The condition that the sum of the inward currents is greater than the sum of the outward currents is necessary for depolarization. However, this does not mean that the system always shows oscillatory behavior [32]. In order to elucidate the mechanisms of I_{Na} mediated EADs, we reduced the model to 3 variables, which are the membrane potential (v), the inactivation gate of the Na channel (h), and the total conductivity of K currents (g_k). The set of ordinary differential equations is

$$\begin{cases} \dfrac{dv}{dt} = -\left(g_{Na} m_\infty^3 h^2 (v - e_{na}) + g_k (v - e_k)\right), \\ \dfrac{dh}{dt} = \dfrac{h_\infty - h}{\tau_h}, \\ \dfrac{dg_k}{dt} = \dfrac{gk_\infty - gk}{\tau_k}, \end{cases}$$

$$gk_\infty = 1 - \exp\left(-3\frac{v + 100}{200}\right),$$

$$\tau_k = 300 \text{ ms}.$$

The first equation shows V_m change due to the simplified currents of I_{Na} and I_K. Inactivation gates h and j are almost identical except for their time constants. Here

http://dx.doi.org/10.1016/j.heliyon.2017.e00388

we reduce them as simply h^2. The smaller τ_h gives faster oscillations. However, the fixed points remain the same. The third equation represents the fact that K currents (I_{Ks}, I_{Kr} etc) increase with time and bring V_m back to the resting V_m. This generic K current was adopted from the simplified model of the cardiac action potential by Echebarria and Karma [33].

This reduced model shows both excitability (i.e. action potential) and oscillatory (i.e. EADs) (Fig. 4A). EADs can be periodic (Fig. 4A), period 2, period 3 (Fig. 4B) and even chaotic (Fig. 4C). Steady state ($-I$) vs. V curves are shown in Fig. 4D. Here we chose ($-I$) instead of I according to standard nonlinear dynamics notation (in contrast to standard electrophysiology nomenclature). If the inward window current is small (red curve), there is only one fixed point (a, filled circle), which is the resting potential of the ventricular cell. This system shows only excitability at the resting potential. As the window current is increased, another fixed point (b, half-filled circle) appears (blue curve) and then, at higher window current, a third fixed point (c, filled circle) appears.

In order to understand the oscillation around the upper fixed point, we consider the two variable system of v and h. Since g_k is the slowest variable of this system, we can identify the behavior of the v-h system for each g_k value using eigenvalues of the v-h system described by the following matrix.

$$\begin{pmatrix} \frac{\partial F}{\partial v} & \frac{\partial F}{\partial h} \\ \frac{\partial G}{\partial v} & \frac{\partial G}{\partial h} \end{pmatrix},$$

where

$$\begin{cases} F = -\left(g_{Na} m_\infty^3 h^2 (v - e_{na}) + g_k (v - e_k)\right), \\ G = \dfrac{h_\infty - h}{\tau_h}, \end{cases}$$

If the eigenvalues of the system are complex, the system of v and h is oscillatory. In other words, having complex eigenvalues is the necessary condition for EADs. In the simplified model, I_K is shown as a straight line (no rectification) in Fig. 4E. At the cross point of this line and $-I_{Na}$ is the stable fixed point (dv/dt = 0, the system does not move from this point). In other words, the outward current is equal to the inward current ($|I_{Na}| = |I_K|$). We compute eigenvalues, which determine the stability of the system, for the fixed point. Depending on the value of g_k, eigenvalues can be real positive, real negative, complex positive, or complex negative. Corresponding biological phenomena are

1) real negative → prolongation of AP without oscillation

2) complex negative → decaying EADs

3) complex positive → growing EADs

http://dx.doi.org/10.1016/j.heliyon.2017.e00388

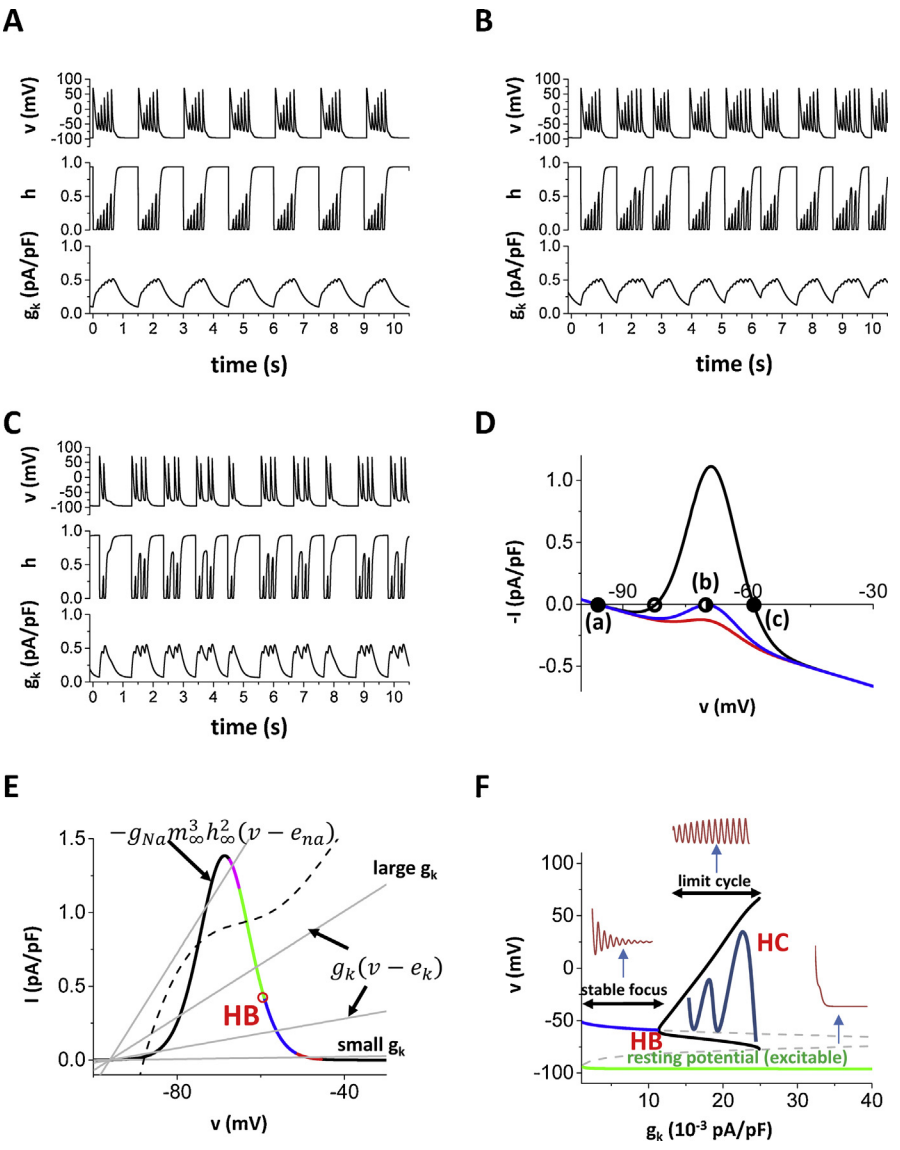

Fig. 4. Eigenvalues and dynamical behaviors. (A) EADs in the simplified 3-variable model. PCL is 1500 ms. (B) Period 3 EADs. (C) Irregular (probably chaotic) EADs. (D) Fixed points. With the normal I_{Na}, the system has only one fixed point (red). As I_{Na} becomes larger (red → blue → black), three fixed points appear. (E) Eigenvalues change as I_K is increased. Red: negative real (e.g. −0.0242 at g_k = 0.001), Blue: negative complex (e.g. −0.005545 ± 0.081 at g_k = 0.01), Green: positive complex (e.g 0.0293 ± 0.09 at g_k = 0.02), Magenta: positive real (e.g. 0.1405 at g_k = 0.04). HB: Hopf bifurcation. Dashed line shows sum of K currents of the physiologically detailed model. (F) Bifurcation diagram. Green line: resting state (stable). The system is always excitable from here. Blue line: stable state (stable focus). Black brunches: maximum and minimum v of the limit cycle. Dashed line: unstable steady state. HB: Hopf bifurcation. HC: homoclinic bifurcation.

4) real positive → repolarization to the resting potential (no EAD)

In Fig. 4E eigenvalues are shown in different colors. If I_K, which is the conductance (g_k) times the driving force ($v - e_k$), is very small, the larger

http://dx.doi.org/10.1016/j.heliyon.2017.e00388

eigenvalue is real negative. In this case, the fixed point is an attractor without oscillations. Since this requires very small I_K, this may not occur physiologically. If I_K is slightly larger (red part), then the eigenvalues are complex negative and the fixed point is an attractor with V_m oscillations (damped EADs) (stable focus). When g_k is included as a third variable, I_K increases as time goes. The eigenvalues become complex positive (green part) from complex negative. At this point (red circle in Fig. 4E and 'HB' in Fig. 4F), Hopf bifurcation occurs and the EAD amplitude grows. As I_K becomes sufficiently large, homoclinic bifurcation occurs ('HC' in Fig. 4F) and V_m goes back to the resting potential.

The I–V curve of the simplified K current is slightly different from the I–V curve of the total K current in the physiological model (Fig. 5). This simplification may affect the results quantitatively but will not qualitatively as far as the I_{Na} exceeds the sum of K currents and Hopf bifurcation occurs. Fig. 5A shows the total K current in the physiologically detailed model. With the normal window current, there is only one fixed point (Fig. 5B dashed line). However, when the window

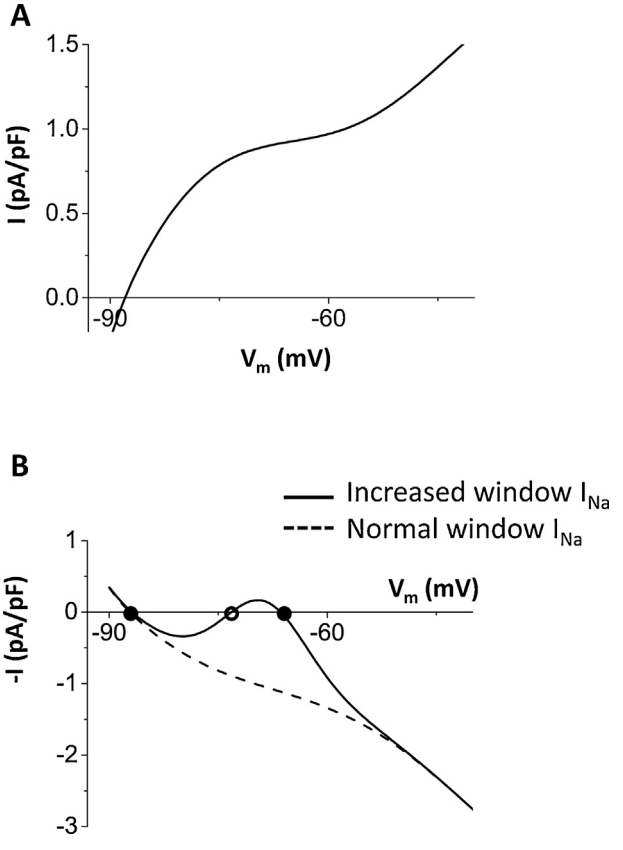

Fig. 5. Fixed points of the physiologically detailed model. (A) The generic K current in the simplified model represents the total K current in the physiological model. Total K current vs voltage. Total K current = $I_{Ks} + I_{Kr} + I_{K1} + I_{to} + I_{NaK}$. (B) Total current vs voltage. Solid line: total current with the increased window I_{Na}. Dashed line: total current with the normal window I_{Na}.

http://dx.doi.org/10.1016/j.heliyon.2017.e00388

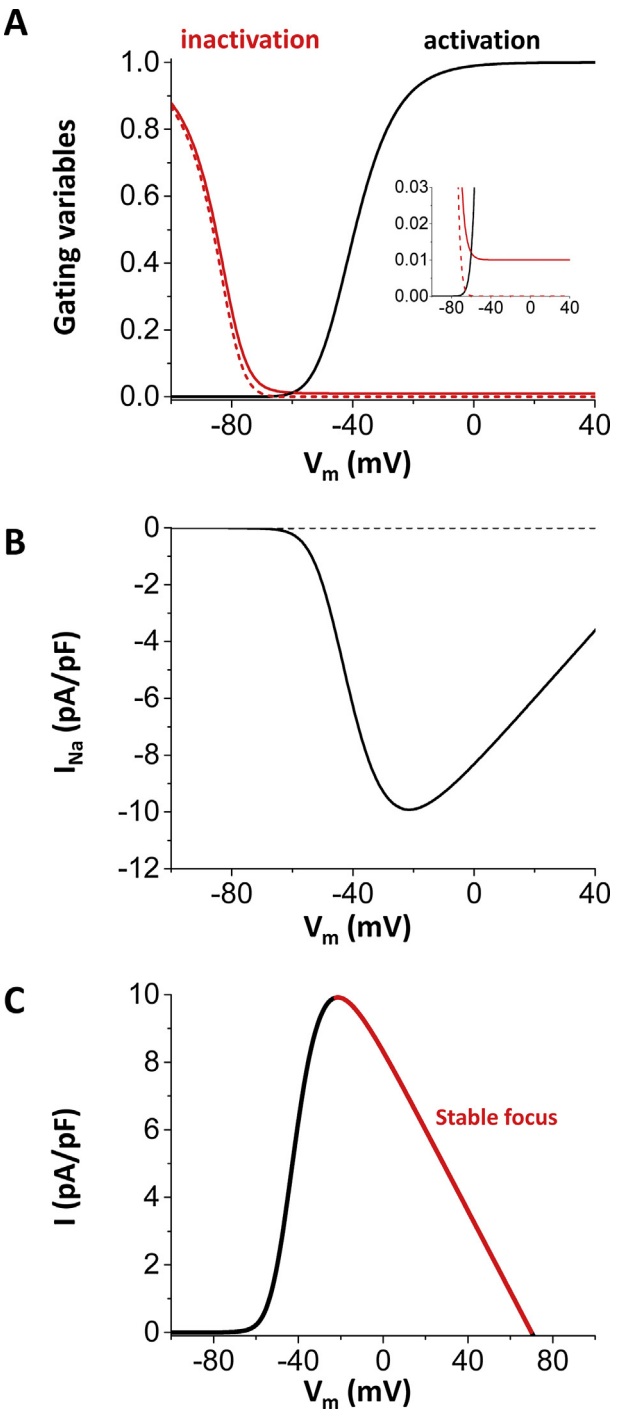

Fig. 6. Non-inactivating I_{Na} does not cause EADs. (A) Activation and inactivation curves. Solid lines: non-inactivating Na channel. Dashed lines: normal Na channel. (B) Steady state current. Solid lines: non-inactivating Na current. Dashed lines: normal Na current. (C) Eigenvalues when the mechanism of the late component of I_{Na} is non-inactivation of the Na channel.

http://dx.doi.org/10.1016/j.heliyon.2017.e00388

current is increased, three fixed points appear (Fig. 5B solid line). EADs in the physiologically detailed model are oscillation around the rightmost fixed point.

Non-inactivation also increases the late component of I_{Na}. However, when the late component of I_{Na} is due to non-inactivating current, although three fixed points can appear, the eigenvalues are always real negative, which indicates no oscillation of V_m (Fig. 6). For example, when 1% of channels are non-inactivating (Fig. 6A), steady state I_{Na} becomes extremely large (Fig. 6B). However, this will not cause EADs since eigenvalues are always real negative (stable focus) although it prolongs the action potential (Fig. 6C).

Therefore, EADs due to reactivation of I_{Na} will not occur in this case although this late component of I_{Na} may set up the conditions for I_{CaL}-mediated EADs by reducing repolarization reserve and EADs due to spontaneous Ca releases by increasing $[Na]_i$, which leads to Ca overload.

3.3. Interplay of I_{Na} and I_{CaL} mediated EADs

In Fig. 2, in order to explore the possibility of I_{Na} mediated EADs, I_{CaL} was blocked. Fig. 7 shows how I_{Na} mediated EADs directly promote I_{CaL} mediated EADs in the presence of I_{Na} and I_{CaL}. Although we cannot say which the cause of EADs is since these are nonlinearly coupled in the system, Fig. 7 clearly shows that reopening of the Na channel precedes reopening of the L-type Ca channel. In this simulation, we used the normal (healthy) L-type Ca channel [25], which is much more difficult to generate EADs than the L-type Ca channel under administration of ISO[32] or H_2O_2 [6]. When V_m became around −70 mV, the Na channel was reactivated first. This caused elevation of V_m, which promoted reactivation of the healthy L-type Ca channel. Ca entry through the L-type Ca channels also helps depolarization via NCX and further promotes EADs.

4. Discussion

In this study, we showed that I_{Na} by itself is able to generate EADs. The dynamical mechanism is oscillation in the I_{Na}-I_K system around the higher V_m fixed point, which is distinguished from the oscillation in the pacemaker cell (oscillation around the single fixed point). I_{Na}, especially the late component of I_{Na} has been recognized as an important player to set up the conditions for EADs by reducing repolarization reserve and increasing intracellular Na concentration, which leads to Ca overload. However, I_{Na} itself has not been considered as a direct initiator of EADs. Under normal conditions, the late component of I_{Na} is so small (Fig. 1B dashed line) that the amplitude of I_{Na} cannot be larger than the sum of K currents at phases 2 and 3, and therefore, I_{Na} itself cannot initiate EADs. However, under pathological conditions such as heart failure [34, 35, 36] and myocardial ischemia [37, 38], large late I_{Na} has been observed. Recent experimental study by Horvath

http://dx.doi.org/10.1016/j.heliyon.2017.e00388

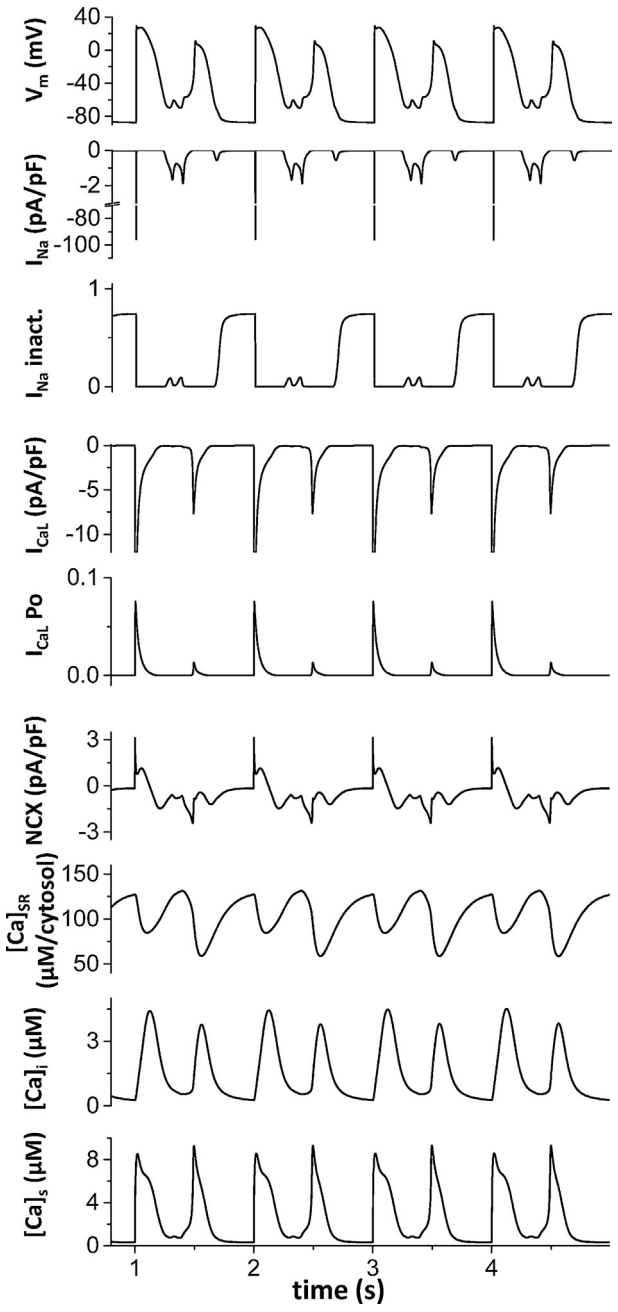

Fig. 7. Interplay of I_{Na} and I_{CaL} mediated EADs. Reactivation of the Na channel promotes reactivation of the L-type Ca channel. Example of EADs when both I_{CaL} and I_{Na} present. The membrane potential, Na current, Na inactivation, L-type Ca current, L-type Ca channel open probability, NCX, SR [Ca], cytosolic [Ca], and submembrane [Ca] are shown. The I_{Na} mediated EADs occurred prior to the I_{CaL} mediated EADs. Ca entry via I_{CaL} also activates NCX and further promotes EADs. Here μM/cytosol means μM v_{sr}/v_i, where v_{sr} is the SR volume and vi is the cell volume.

et al. showed that I_{Na} is as large (~1 pA/pF) as the other Ca and K currents. We reconstructed I_{Na} based on activation and inactivation curves (Fig. 1A) measured by Wang et al. and the amplitude of I_{Na} predicted by the model gives similar

http://dx.doi.org/10.1016/j.heliyon.2017.e00388

amplitude (Fig. 1B solid line). This implies that I_{Na} may overcome the sum of I_K and depolarize V_m during AP without the help of the other inward currents such as I_{CaL}, NCX, non-specific Ca-activated cation current, especially, when I_K become small under pathological conditions and/or administration of K channel blockers. Using the physiologically detailed model of the ventricular action potential, we showed I_{Na} mediated EADs (Fig. 2). As we have shown in I_{CaL}-mediated EADs [6], I_{Na}-mediated EADs can be periodic (Fig. 2A), period-2 (Fig. 2B), and even chaotic (Fig. 2C).

We have shown the mechanisms of I_{CaL}-mediated EADs [32, 39]. Also, bursting behaviors are widely observed and studied in many biological systems [20, 21, 22]. In this study, we reduced the physiologically detailed model to the 3-variable model and analyzed the dynamical mechanism of I_{Na} mediated EADs. This methodology has been used in theoretical neuroscience to understand underlying mechanisms [22, 40]. We have also used this type of analysis for I_{CaL}-mediated EADs [32, 39]. For the formation of EADs, positive feedback processes such as I_{CaL} or Ca induced Ca release from the SR are necessary. In addition to them, I_{Na} has a positive feedback process since more Na channels open as V_m elevates. In this study, we showed I_{Na}-mediated EADs due to the Na channel reactivation. The EAD, namely the oscillation of V_m at phases 2 and/or 3, in this case is distinguished from the V_m oscillation in the pacemaker cell [23, 24]. In the model of the voltage clock of the pacemaker cell, the system has only one fixed point, which is unstable, gives V_m oscillation. On the other hand, the model shown in this study has three fixed points as the window current is increased. I_{Na} mediated EADs are due to oscillation around the higher V_m fixed point. The lower fixed point (the resting potential) is still stable and the system shows excitability.

The Na channel can reactivate without large window current if there is another positive feedback mechanism, which helps reactivation of the Na channel. For example, Edward et al. have shown that reactivation of Na channel when SR Ca release occurs [41, 42]. In these cases, the higher V_m fixed point is not necessary. Stimulation such as spontaneous SR Ca release via NCX activates the Na channel from the lower V_m fixed point.

The sustained Na current can also be due to non-inactivation of the Na channel. However, our analysis shows that AP will be simply prolonged and EADs will not occur (Fig. 6) in this case. The prolongation of AP without EADs is also observed with late component of the Na current experimentally [19]. In this case, although the Na channel will not reactivate, prolongation can promote I_{CaL}-mediated EADs and Ca overload.

In order to increase the window current, activation and inactivation curves are shifted. The amplitude of the upstroke of AP becomes larger since activation occurs at the lower potential and inactivation requires higher potential. Zhao et al.

http://dx.doi.org/10.1016/j.heliyon.2017.e00388

have shown that smaller amplitude of the upstroke promotes EADs [43]. In our case, the amplitude is smaller with the normal I_{Na}. However, there is only one fixed point with the normal I_{Na} (Fig. 4D red curve, Fig. 5 dashed curve). Therefore, even if the amplitude of the upstroke is smaller, EADs will not occur with the normal I_{Na} unless K currents are unphysiologically small.

In the case of I_{CaL}-mediated EADs, I_{CaL} is responsible only for oscillation at phases 2 and/or 3. On the other hand, in the case of I_{Na}-mediated EADs, I_{Na} is responsible for both excitation and oscillation. In addition, I_{CaL}-mediated EADs occur around $-20 \sim 10$ mV. In some experiments, EADs are observed at more negative V_m than the reactivation V_m of the L-type Ca channel [42, 44]. Damiano and Rosen observed more EADs as the PCL becomes longer [44]. As the PCL becomes longer, SR Ca load becomes smaller and EADs due to spontaneous Ca releases occur less in large mammalian ventricular cells. Therefore, if the mechanism of EADs is due to spontaneous Ca releases, EADs should occur less as the PCL becomes longer. In addition, if the mechanism of EADs is due to reactivation of the L-type Ca channel, EADs should occur at more positive voltage. This experimental observation suggests that these EADs are due to Na channel reactivation and consistent with our results (Fig. 2, more EADs with longer PCLs). Our mechanism may explain these EADs although we need additional experiments to differentiate them more explicitly from EADs caused by the other mechanisms.

Recently, the current through the Nav1.8 channel has been considered to be a possible mechanism of I_{NaL} in cardiac cells [45, 46]. This channel also has a positive feedback process like Nav1.5 and would similarly cause I_{Na} mediated EADs. However, EADs would occur a much higher V_m range, because for Nav1.8 the window current V_m range is closer to that of the L-type Ca channel [45].

Declarations

Author contribution statement

Daisuke Sato: Conceived and designed the experiments; Performed the experiments; Analyzed and interpreted the data; Contributed reagents, materials, analysis tools or data; Wrote the paper.

Colleen E. Clancy, Donald M. Bers: Conceived and designed the experiments; Analyzed and interpreted the data; Contributed reagents, materials, analysis tools or data; Wrote the paper.

Competing interest statement

The authors declare no conflict of interest.

http://dx.doi.org/10.1016/j.heliyon.2017.e00388

Funding statement

This work was supported by National Institutes of Health grant K99/R00-HL111334, American Heart Association Grant-in-Aid 16GRNT31300018, and Amazon AWS Cloud Credits for Research (D.S.), National Institutes of Health grants U01-HL126273 and R01-HL128170 (C.E.C.), and National Institutes of Health grants R37-HL30077 and R01-HL105242 (D.M.B.)

Additional Information

No additional information is available for this paper.

References

[1] D.W. Frazier, P.D. Wolf, J.M. Wharton, A.S. Tang, W.M. Smith, R.E. Ideker, Stimulus-induced critical point. Mechanism for electrical initiation of reentry in normal canine myocardium, J. Clin. Invest. 83 (3) (1989) 1039–1052 PubMed PMID: 2921316; PMCID: 303781.

[2] B. Rodriguez, L. Li, J.C. Eason, I.R. Efimov, N.A. Trayanova, Differences between left and right ventricular chamber geometry affect cardiac vulnerability to electric shocks, Circ. Res. 97 (2) (2005) 168–175 PubMedPMID: 15976315; PMCID: 2925187.

[3] F.G. Akar, D.S. Rosenbaum, Transmural electrophysiological heterogeneities underlying arrhythmogenesis in heart failure, Circ. Res. 93 (7) (2003) 638–645 PubMed PMID: 12933704.

[4] E. Patterson, W.M. Jackman, K.J. Beckman, R. Lazzara, D. Lockwood, B.J. Scherlag, R. Wu, S. Po, Spontaneous pulmonary vein firing in man: relationship to tachycardia-pause early afterdepolarizations and triggered arrhythmia in canine pulmonary veins in vitro, J. Cardiovasc. Electrophysiol. 18 (10) (2007) 1067–1075 PubMed PMID: 17655663.

[5] A. Burashnikov, C. Antzelevitch, Reinduction of atrial fibrillation immediately after termination of the arrhythmia is mediated by late phase 3 early afterdepolarization-induced triggered activity, Circulation 107 (18) (2003) 2355–2360 PubMed PMID: 12695296.

[6] D. Sato, L.H. Xie, A.A. Sovari, D.X. Tran, N. Morita, F. Xie, H. Karagueuzian, A. Garfinkel, J.N. Weiss, Z. Qu, Synchronization of chaotic early afterdepolarizations in the genesis of cardiac arrhythmias, Proc. Natl. Acad. Sci. U. S. A. 106 (9) (2009) 2983–2988 PubMed PMID: 19218447; PMCID: 2651322.

 http://dx.doi.org/10.1016/j.heliyon.2017.e00388

[7] C.T. January, A. Moscucci, Cellular mechanisms of early afterdepolarizations, Ann. N.Y. Acad. Sci. 644 (1992) 23–32 PubMed PMID: 1562117.

[8] W.T. Clusin, Calcium and cardiac arrhythmias: DADs, EADs, and alternans, Crit. Rev. Clin. Lab. Sci. 40 (3) (2003) 337–375 PubMed PMID: 12892319.

[9] P.G. Volders, M.A. Vos, B. Szabo, K.R. Sipido, S.H. de Groot, A.P. Gorgels, H.J. Wellens, R. Lazzara, Progress in the understanding of cardiac early afterdepolarizations and torsades de pointes: time to revise current concepts, Cardiovasc. Res. 46 (3) (2000) 376–392 PubMed PMID: 10912449.

[10] J. Zeng, Y. Rudy, Early afterdepolarizations in cardiac myocytes: mechanism and rate dependence, Biophys. J. 68 (3) (1995) 949–964 PubMed PMID: 7538806; PMCID: 1281819.

[11] B.R. Choi, F. Burton, G. Salama, Cytosolic Ca2+ triggers early afterdepolarizations and Torsade de Pointes in rabbit hearts with type 2 long QT syndrome, J. Physiol. 543 (Pt 2) (2002) 615–631 PubMed PMID: 12205194; PMCID: 2290501.

[12] D. Guo, X. Zhao, Y. Wu, T. Liu, P.R. Kowey, G.X. Yan, L-type calcium current reactivation contributes to arrhythmogenesis associated with action potential triangulation, J. Cardiovasc. Electrophysiol. 18 (2) (2007) 196–203 PubMed PMID: 17212595.

[13] C.I. Spencer, J.S. Sham, Effects of Na+/Ca2+ exchange induced by SR Ca2+ release on action potentials and afterdepolarizations in guinea pig ventricular myocytes, Am. J. Physiol. Heart Circ. Physiol. 285 (6) (2003) H2552–62 PubMed PMID: 12933341.

[14] H.A. Fozzard, D.A. Hanck, Structure and function of voltage-dependent sodium channels: comparison of brain II and cardiac isoforms, Physiol. Rev. 76 (3) (1996) 887–926 PubMed PMID: 8757791.

[15] J.M. Nerbonne, R.S. Kass, Molecular physiology of cardiac repolarization, Physiol. Rev. 85 (4) (2005) 1205–1253 PubMed PMID: 16183911.

[16] W. Song, W. Shou, Cardiac sodium channel Nav1.5 mutations and cardiac srrhythmia, Pediatr. Cardiol. 33 (6) (2012) 943–949 PubMed PMID: PMC3393812.

[17] X.H. Wehrens, T. Rossenbacker, R.J. Jongbloed, M. Gewillig, H. Heidbuchel, P.A. Doevendans, M.A. Vos, H.J. Wellens, R.S. Kass, A novel mutation L619F in the cardiac Na+ channel SCN5A associated with long-QT syndrome (LQT3): a role for the I-II linker in inactivation gating, Hum. Mutat. 21 (5) (2003) 552 Epub 2003/04/04. PubMed PMID: 12673799.

 http://dx.doi.org/10.1016/j.heliyon.2017.e00388

[18] A.J. Horne, J. Eldstrom, S. Sanatani, D. Fedida, A novel mechanism for LQT3 with 2:1 block: a pore-lining mutation in Nav1.5 significantly affects voltage-dependence of activation, Heart Rhythm 8 (5) (2011) 770–777.

[19] B. Horvath, T. Banyasz, Z. Jian, B. Hegyi, K. Kistamas, P.P. Nanasi, L.T. Izu, Y. Chen-Izu, Dynamics of the late Na(+) current during cardiac action potential and its contribution to afterdepolarizations, J. Mol. Cell Cardiol. 64 (2013) 59–68 PubMed PMID: 24012538; PMCID: 3856763.

[20] X.-J. Wang, J. Rinzel, Oscillatory and bursting properties of neurons, Michael A.A., MIT Press, The handbook of brain theory and neural networks, 1998, pp. 686–691.

[21] J. Rinzel, Bursting Oscillations in an Excitable Membrane Model. Ordinary and Partial Differential Equations, Springer, 1985, pp. 304–316.

[22] E.M. Izhikevich, Dynamical Systems in Neuroscience, MIT press, 2007.

[23] Y. Kurata, H. Matsuda, I. Hisatome, T. Shibamoto, Regional difference in dynamical property of sinoatrial node pacemaking: role of na+ channel current, Biophys. J. 95 (2) (2008) 951–977 PubMed PMID: 18390617; PMCID: 2440451.

[24] B. van der Pol, J.M. van der Mark XXII, The heartbeat considered as a relaxation oscillation, and an electrical model of the heart, Lond. Edinb. Dublin Philos. Mag. J. Sci. 6 (38) (1928) 763–775.

[25] A. Mahajan, Y. Shiferaw, D. Sato, A. Baher, R. Olcese, L.H. Xie, M.J. Yang, P.S. Chen, J.G. Restrepo, A. Karma, A. Garfinkel, Z. Qu, J.N. Weiss, A rabbit ventricular action potential model replicating cardiac dynamics at rapid heart rates, Biophys. J. 94 (2) (2008) 392–410 PubMedPMID: 18160660; PMCID: 2157228.

[26] D.W. Wang, K. Yazawa, A.L. George Jr., P.B. Bennett, Characterization of human cardiac Na+ channel mutations in the congenital long QT syndrome, Proc. Natl. Acad. Scie. U. S. A. 93 (23) (1996) 13200–13205 PubMed PMID: 8917568; PMCID: 24070.

[27] C.H. Luo, Y. Rudy, A model of the ventricular cardiac action potential. Depolarization, repolarization, and their interaction, Circ. Res. 68 (6) (1991) 1501–1526 PubMed PMID: 1709839.

[28] C.H. Luo, Y. Rudy, A dynamic model of the cardiac ventricular action potential. I. Simulations of ionic currents and concentration changes, Circ. Res. 74 (6) (1994) 1071–1096 PubMed PMID: 7514509.

 http://dx.doi.org/10.1016/j.heliyon.2017.e00388

[29] T.R. Shannon, F. Wang, J. Puglisi, C. Weber, D.M. Bers, A mathematical treatment of integrated Ca dynamics within the ventricular myocyte, Biophys. J. 87 (5) (2004) 3351–3371 PubMed PMID: 15347581; PMCID: 1304803.

[30] A. Zaza, M. Rocchetti, The late Na+ current-origin and pathophysiological relevance, Cardiovasc. Drugs Ther. 27 (1) (2013) 61–68 PubMed PMID: 23274937 ; PMCID: 3555240.

[31] V.A. Maltsev, H.N. Sabbah, R.S. Higgins, N. Silverman, M. Lesch, A.I. Undrovinas, Novel, ultraslow inactivating sodium current in human ventricular cardiomyocytes, Circulation 98 (23) (1998) 2545–2552 PubMed PMID: 9843461.

[32] Y. Xie, L.T. Izu, D.M. Bers, D. Sato, Arrhythmogenic transient dynamics in cardiac myocytes, Biophys. J. 106 (6) (2014) 1391–1397 PubMed PMID: 24655514; PMCID: 3984988.

[33] B. Echebarria, A. Karma, Mechanisms for initiation of cardiac discordant alternans, Eur. Phys. J. Spec. Top. 146 (1) (2007) 217–231.

[34] R. Coppini, C. Ferrantini, L. Yao, P. Fan, M. Del Lungo, F. Stillitano, L. Sartiani, B. Tosi, S. Suffredini, C. Tesi, M. Yacoub, I. Olivotto, L. Belardinelli, C. Poggesi, E. Cerbai, A. Mugelli, Late sodium current inhibition reverses electromechanical dysfunction in human hypertrophic cardiomyopathy, Circulation 127 (5) (2013) 575–584 PubMed PMID: 23271797.

[35] M. Pourrier, S. Williams, D. McAfee, L. Belardinelli, D. Fedida, CrossTalk proposal: the late sodium current is an important player in the development of diastolic heart failure (heart failure with a preserved ejection fraction), J. Physiol. 592 (Pt 3) (2014) 411–414 PubMed PMID: 24488066; PMCID: 3930422.

[36] A.I. Undrovinas, L. Belardinelli, N.A. Undrovinas, H.N. Sabbah, Ranolazine improves abnormal repolarization and contraction in left ventricular myocytes of dogs with heart failure by inhibiting late sodium current, J. Cardiovasc. Electrophysiol. 17 (Suppl. 1) (2006) S169–S177 PubMed PMID: 16686675; PMCID: 1482456.

[37] L.S. Maier, S. Sossalla, The late Na current as a therapeutic target: where are we? J. Mol. Cell. Cardiol. 61 (2013) 44–50 PubMed PMID: 23500390.

[38] L. Belardinelli, J.C. Shryock, H. Fraser, The mechanism of ranolazine action to reduce ischemia-induced diastolic dysfunction, Eur. Heart J. Suppl. 8 (Suppl. A) (2006) A10–A13 2006-02-01.

 http://dx.doi.org/10.1016/j.heliyon.2017.e00388

[39] D.X. Tran, D. Sato, A. Yochelis, J.N. Weiss, A. Garfinkel, Z. Qu, Bifurcation and chaos in a model of cardiac early afterdepolarizations, Phys. Rev. Lett. 102 (25) (2009) 258103 PubMed PMID: 19659123; PMCID: 2726623.

[40] N.I. Krouchev, F. Rattay, M. Sawan, A. Vinet, From squid to mammals with the HH model through the nav channels' half-activation-voltage parameter, PloS One 10 (12) (2015) e0143570 Eub 2015/12/03. PubMed PMID: 26629692; PMCID: PMC4667926.

[41] S. Morotti, A.D. McCulloch, D.M. Bers, A.G. Edwards, E. Grandi, Atrial-selective targeting of arrhythmogenic phase-3 early afterdepolarizations in human myocytes, J. Mol. Cell. Cardiol. 96 (2016) 63–71 Epub 2015/08/05. PubMed PMID: 26241847; PMCID: PMC4734906.

[42] A.G. Edwards, E. Grandi, J.E. Hake, S. Patel, P. Li, S. Miyamoto, J.H. Omens, J. Heller Brown, D.M. Bers, A.D. McCulloch, Nonequilibrium reactivation of Na+ current drives early afterdepolarizations in mouse ventricle, Circ. Arrhythm. Electrophysiol. 7 (6) (2014) 1205–1213 PubMedPMID: 25236710; PMCID: 4301603.

[43] Z. Zhao, Y. Xie, H. Wen, D. Xiao, C. Allen, N. Fefelova, W. Dun, P.A. Boyden, Z. Qu, L.H. Xie, Role of the transient outward potassium current in the genesis of early afterdepolarizations in cardiac cells, Cardiovasc. Res. 95 (3) (2012) 308–316 Epub 2012/06/05. PubMed PMID: 22660482; PMCID: PMC3400356.

[44] B.P. Damiano, M.R. Rosen, Effects of pacing on triggered activity induced by early afterdepolarizations, Circulation 69 (5) (1984) 1013–1025 PubMed PMID: 6705157.

[45] T. Yang, T.C. Atack, D.M. Stroud, W. Zhang, L. Hall, D.M. Roden, Blocking Scn10a channels in heart reduces late sodium current and is antiarrhythmic, Circ. Res. 111 (3) (2012) 322–332 PubMed PMID: 22723299; PMCID: 3412150.

[46] E. Savio-Galimberti, P. Weeke, R. Muhammad, M. Blair, S. Ansari, L. Short, T.C. Atack, K. Kor, C.G. Vanoye, M.S. Olesen, Yang T LuCamp, A.L. George Jr., D.M. Roden, D. Darbar, SCN10A/Nav1.8 modulation of peak and late sodium currents in patients with early onset atrial fibrillation, Cardiovasc. Res. (2014) PubMed PMID: 25053638.

 http://dx.doi.org/10.1016/j.heliyon.2017.e00388